On the Role of the North Equatorial Counter Current in Transporting Heat during a Strong El Niño

David J. Webb

National Oceanography Centre, Southampton SO14 3ZH, U.K.

Correspondence to: D.J.Webb (djw@noc.ac.uk)

Abstract. An analysis of archived data from the Nemo 1/12th degree global ocean model shows the importance of the NECC in the development of the 1982-83 El Niño. The model results indicate that heat transport by the NECC is usually restricted by a combination of Ekman transport, geostrophic inflow and tropical instability waves. During the development of an El Niño these may be reduced near to and to the west of the region of increased atmospheric convection in the Pacific. This allows
5   increased heat transport eastwards by the NECC which in turn may move the atmospheric convection further east across the Pacific Ocean.

1   Introduction

Studies of the Tropical Pacific often focus on the Equatorial Waveguide and the propagation of equatorial Kelvin waves generated by wind events (i.e. Levine and McPhaden, 2016; Chen et al., 2016; Hu and Fedorov, 2017). The study reported here
10   starts in a similar manner using data from a long run of the Nemo 1/12th degree computer model of the global ocean. Average surface temperatures in the equatorial band of the Pacific are plotted as a function of longitude and time. During the strong El Niño events of 1982-83 and 1997-98 the figure shows warm events propagating eastwards from the Warm Pool region of the West Pacific across to the South American coastline. Similar events are seen in other years but these stop in the Central Pacific around 220°E (130°W).

15   The warm events propagate eastwards at a speed of about $0.6 \, \mathrm{m \, s^{-1}}$. The Equatorial Pacific is highly stratified, with the warmest water concentrated in the top $200 \, \mathrm{m}$, so a speed of $0.6 \, \mathrm{m \, s^{-1}}$ is comparable with the speed of a number of equatorial Kelvin wave modes whose first zero occurs similarly at around $200 \, \mathrm{m}$. There is therefor some justification in connecting the propagation of the warm features with the propagation of equatorial Kelvin waves.

Except that this is highly unlikely. Simple waves, like equatorial Kelvin waves, transport momentum and energy but they
20   cannot easily transport quantities like temperature and salinity, qualities associated with individual particles in the medium. Such advection can only occur if the waves are highly non-linear so that particle velocities are comparable with the phase velocity. This occurs in breaking waves and, to a lesser extent, in tidal bores but, as far as the author is aware, no one has reported evidence for an equivalent major feature in the near-surface layers of the Equatorial Pacific.

In order to clarify the situation, model archived data is used to calculate the flux of warm water across 180°E and 240°E as
25   a function of time during the period 1980 to 1985. This period includes the strong 1982-1983 El Niño. The calculation shows
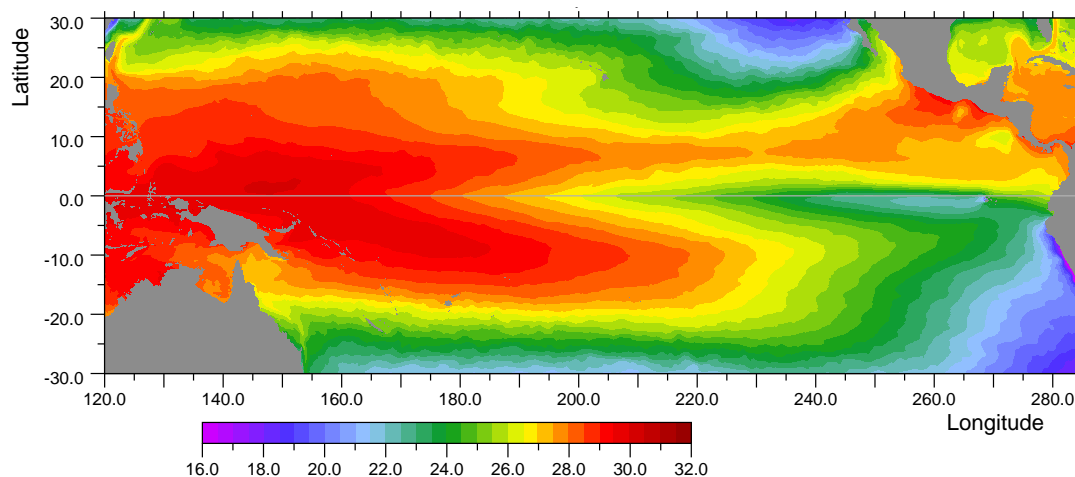
Figure 1. Average Sea Surface Temperature (°C) of the Equatorial Pacific region of the model during 1981.

that during the El Niño, the main flux of warm water in the model did not occur within the Equatorial Waveguide. Instead it occurs further north, at the latitude of the eastward flowing North Equatorial Counter Current (NECC).

Wyrtki (1973, 1974) was possibly the first to suggest that the NECC had the potential to transport significant amounts of heat eastwards in the Tropical Pacific. The NECC continues to be important in his later papers (i.e. Wyrtki, 1977, 1979) but in

5 his theory for the El Niño (Wyrtki, 1975) he also introduced the idea of equatorial Kelvin waves triggering the El Niño. It is this aspect of his work that has been developed most by later authors.

To return to the NECC, the model results studied here indicate that in most years the Ekman transport, the geostrophic inflow and tropical instability waves carry warm water away from the core of the NECC and replace it with cooler water from the north and south. As a result the core temperature of the NECC is significantly reduced.

10 During periods when an El Niño is developing, the region of low zonal wind stress moves eastwards across the ocean. (This region generally lies near the centre of a much larger area of increased atmospheric convection). The model shows that one result of the low winds is that at the longitudes affected, the Ekman transport at the latitude of the NECC is reduced. The strength of the geostrophic inflow is also reduced as is the strength of the tropical instability waves. The latter is probably in part due to the reduction and change in direction of the surface current at the Equator.

15 As a consequence, while the El Niño develops, the NECC transports much warmer water than normal past the region of low winds. This transport of warm water occurs near the latitudes of the subtropical convergence in the atmosphere. Thus although the present study does not include an atmospheric model, it is hypothesized that it is this warmer water which moves the region of increased atmospheric convection and the area of low winds further east. The process is the repeated, moving the convection region, the region of low winds and warmer than normal water, steadily eastwards across the ocean.
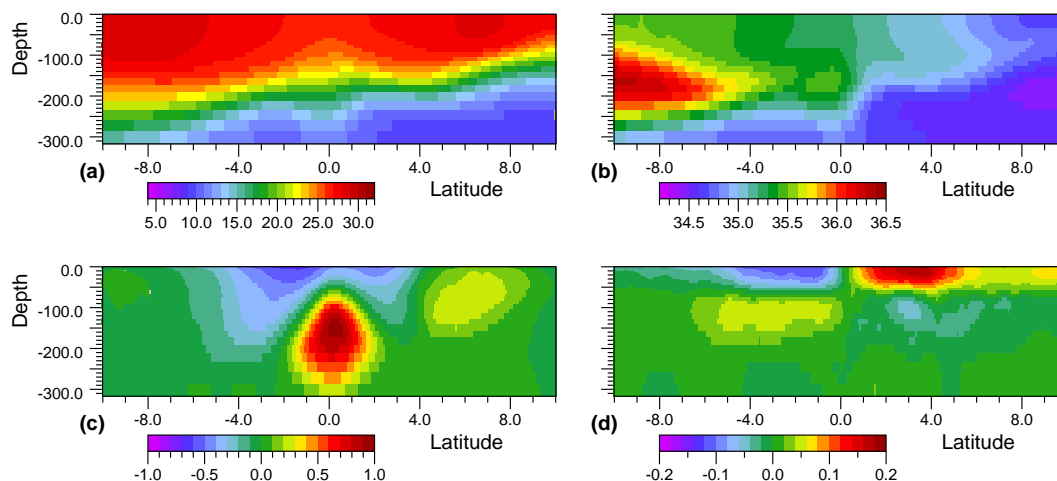
Figure 2. North-South Sections at 200°E (160°W) of the average values during 1981 of (a) temperature (°C), (b) salinity, and (c) east and (d) north components of velocity ($\mathrm{m\,s^{-1}}$).

Further support for this argument is obtained by tracing particles during a strong El Niño and a non-El Niño year. The results from the model show that during the non-El Niño year, water particles are rapidly mixed out of the NECC but during the strong El Niño year they stay within the NECC and are transported further to the east.

The analysis also shows that the strength of the NECC is affected by annual Rossby waves which propagate westwards across the Equatorial Pacific. It is found that the wave at 6°N, arrives in the Western Pacific in mid-year and has the effect of increasing the strength of the NECC at that time. In 1982 the amplitude of the wave in the Western Pacific was greater than normal and this may have contributed to the development of a stronger than normal El Niño during the 1982-83 period.

Although Nemo is only a computer model and all models have errors, on the basis of these results it is argued that the following five hypotheses are true. First it is hypothesised that, for the real ocean, Wyrtki was correct and that the NECC can transport significant amounts of heat. Secondly it is hypothesized that, in a normal year, the transport of heat by the NECC is reduced by Ekman transport, the geostrophic inflow and tropical instability waves. Thirdly it is hypothesised that, in an El Nino year, these processes are themselves reduced at the longitude of the low wind stress region and at longitudes west of this point.

Fourthly it is hypothesised that the resulting increased heat transport by the current results in an eastward progression of both the region of warmer than normal water and the region of strong atmospheric convection. Finally it is hypothesised that the year to year variations in the strength of the NECC are responsible for much of the variability in the strength of El Niños.

As such these hypotheses are in conflict with the more traditional El Niño theory in which westerly wind bursts generate the equatorial Kelvin waves. The model does indeed capture such events in late 1982, but the timing is such that they appear to be a response to the El Niño rather than its cause.

2 The Nemo 1/12° global ocean model

The ocean model discussed here is one of the family of Nemo models (Madec, 2014), all with a similar code base but with different choices of horizontal and vertical grid resolution and of the many options for representing the underlying ocean physics. The present model uses a non-uniform grid based on a longitude grid spacing of 1/12° along the Equator. In the

5   Southern Hemisphere and in the Indian and Pacific Oceans the latitude spacing is chosen so that each of the grid boxes has the same width and height. In the North Atlantic and Arctic a more complex scheme is used to prevent the convergence of the grid near the pole.

The model has 75 layers in the vertical. Their nominal thicknesses range from 1 m at the surface to 204 m in the lowest layer but as the ocean surface moves up and down each of the layers expands or contracts slightly to allow for this. The nominal

10   thicknesses are based on an analytic formula which ensures a smooth transition between the strongly stratified surface layers, which need to be well resolved, and the weakly stratified deep ocean for which less resolution is necessary. One result of this is that 35 layers are used to resolve just the top 300 m. In the Equatorial Pacific this covers most of the major current systems.

The surface boundary conditions used for run 6 of the high resolution model, discussed here, are those of Large and Yeager (2004) together with the Drakker DFS5.2 atmospheric fields described by Dussin et al. (2014). The Drakkar datasets, like the

15   ECMWF reanalysis datasets on which they are based, start from 1958. This is also the start date of run 6.

In a previous analysis of run 6, Webb (2016) compared observed temperatures in the Equatorial Pacific Niño regions with those from the model. The Niño regions are a series of standard ocean areas in the Equatorial Pacific often used in El Niño studies (Trenberth, 1997).

The analysis of sea surface temperatures in the Niño regions, showed that there was good agreement between observations

20   and the model. It also showed that this was not due to the existence of a strong feedback loop - the actual sea surface temperature somehow controlling the model SST via its effect of the atmosphere layers closest to the ocean surface. On the basis of these results it appears reasonable to make further use of the model archive data in the present study of processes affecting the El Niño.

Data from the model is available in the form of averages over each five-day period during the model run. The analysis

25   reported here concentrates on 1981, as a typical non-El Niño year, and on the 1982-83 period, during which a strong El Niño developed.

As background, Fig.1 shows the model average sea surface temperature (SST) during 1981. In the west the North Pacific Warm Pool shows a large region with average temperatures above 28°C. Similar temperatures are also found over a large region of the South Pacific. The figure also shows the region of the Equatorial Waveguide, extending from 5°S to 5°N, which

30   is analysed in the next section of this paper. In the west this has average temperatures above 28°C, but in the east, where the Equatorial Undercurrent outcrops temperatures fall below 23°C.

Figure 2 shows the average values of temperature, salinity and velocity near the surface in a section at 200°E (160°W). The figure illustrates the strong stratification of the surface layers and the fact that the primary currents of the region, the Equatorial Current, the Equatorial Undercurrent and the North Equatorial Counter Current all lie close to the ocean surface.

The archive datasets also contain the ocean surface wind stress and precipitation fields used to force the model. The wind stress field shows that, during the development of the 1982-82 El Niño, a major feature was a region of low wind stress. This first formed to the east of New Guinea and then moved eastwards along the equator, reaching 220°E (140°W) by the end of the year. It was also an area of high surface ocean temperatures.

5   The low wind stress region can be seen in Figs. 21 to 24. Its development can be followed in Fig 17, which shows the wind stress at the Equator. The forcing data shows that usually there is little precipitation within the low wind stress region, indicating that it is not an area of strong atmospheric convection. However it is surrounded by bands of strong wind stress convergence and these are usually close to regions with high rates of precipitation.

To show how this changes in time, Fig. 25 plots the average precipitation rate between 12°S and 12°N, plotted as a function 10 of longitude and time. The figure confirms that the El Niño is associated with enhanced precipitation rates in the Central Pacific.

In the South Pacific, precipitation may be enhanced by the South Pacific Warm Pool, especially late in the year after the Sun has crossed the Equator. Precipitation also increases in the Eastern Pacific, along the line of the ITCZ, but as only a small latitude band is involved the net contribution of any increase may be small.

3   Time series of mean temperatures in the equatorial band

15 In the standard picture of an El Niño, warm water from the Western Pacific moves to the Central Equatorial Pacific and, in the more extreme cases all the way to the South American Coastline. This warming of the Central and Eastern Pacific moves the location of the dominant atmospheric convection region eastwards and, because of the amount of heat energy involved, results in large scale changes in the atmospheric circulation.

Figure 3 plots the sea surface temperature, averaged between 5°S and 5°N, as a function of longitude and for the period 1980 20 to 2000. During the whole of this period temperatures in the Western Equatorial Pacific hover around 30°C but in the Eastern Pacific the mean temperature can vary between 22°C and 30°C. The longest periods of warm temperatures occur during the strong El Niño events of 1982-83 and 1997-98, but short periods with temperatures above 28°C also occur in 1987, 1992 and 1993.

The period between 1980 and 1985 is expanded in Fig. 4, together with a similar figure for the period including the 1997/98 25 El Niño, emphasising the similarities between the two strong El Ninos. The third figure comes from a similar period from a fully coupled run, where the same ocean model was coupled to a high resolution atmospheric model. In this case the ocean temperatures are slightly too low, but it shows that the detailed structures seen in the figures are not the result of forcing by, possibly anomalous, surface boundary conditions but arise as natural variabilities of the coupled system.

As well as the main El Niño event, each of the figures show a series of fine scale wave-like features, with an east-west 30 wavelength of five to ten degrees and a period of about a month. The features grow in amplitude during the Autumn of each year and die out in the Spring when their westward phase velocity tends to be reduced or even reversed. Their wavelength and period is consistent with them being due to the passage of tropical instability waves (TIWs). As each TIW passes it advects
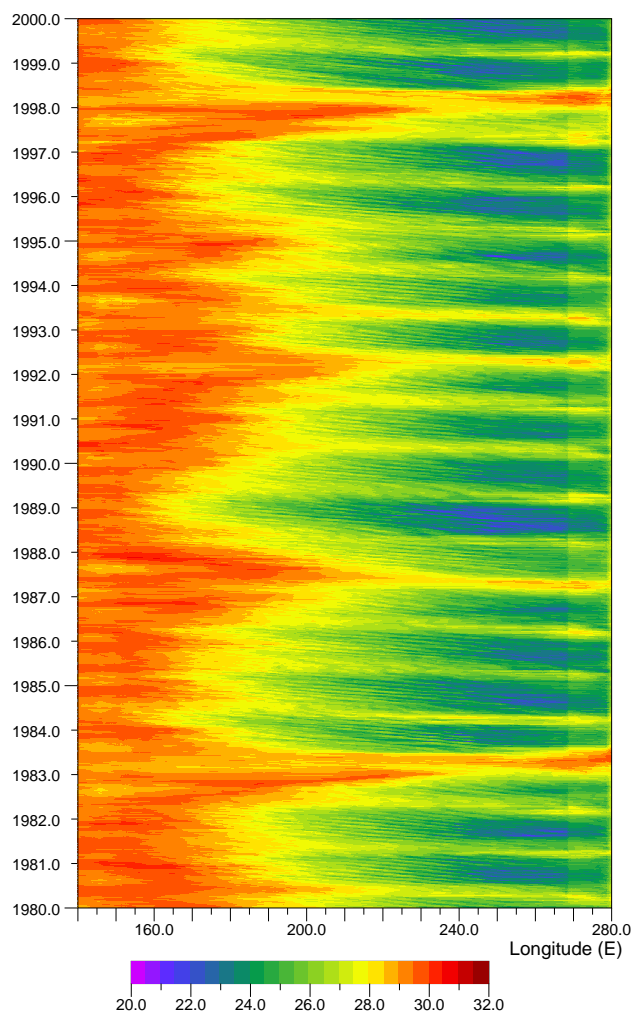
Figure 3. Average model sea surface temperature (°C) in the Equatorial Pacific between 5°S and 5 °N, plotted for longitudes 120°E to 280°E (80°W) and years 1980.0 to 2000.0.

warm water into the equatorial band but after it has passed upwelling at the Equator will return the sea surface temperature to its earlier value.

The second feature of note is the annual signal which primarily affects the Eastern and Central Pacific. Near the South American coastline, temperatures are at a maximum early each year, a comparison with the wind field (i.e. Fig 17) indicating

5   that this occurs after periods when the eastward component of the wind stress has dropped to near zero. Thus they are probably partly due to a reduction in equatorial upwelling but as the wind field is very noisy the evidence for this is weak. Further west the period of low winds occurs later and this may explain why the temperature maximum in the annual signal occurs later towards the Central Pacific.
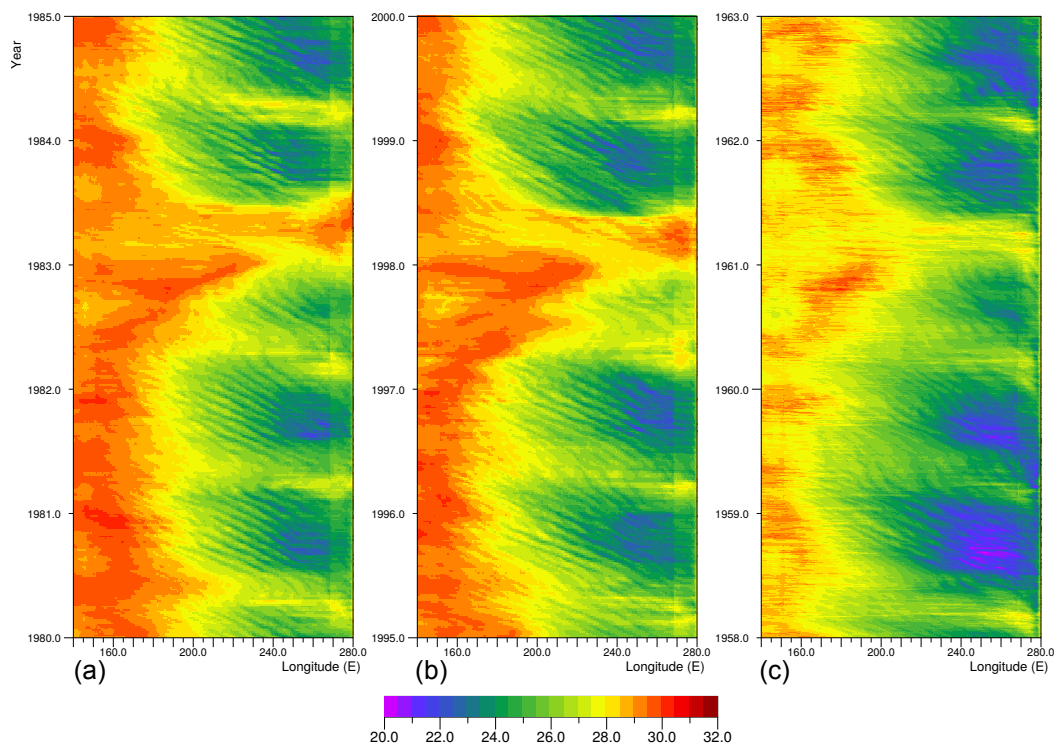
Figure 4. Expanded view of model sea surface temperature, averaged between 5°S and 5 °N, for the Equatorial Pacific between 120°E and 280°E (80°W), and (a) between 1980 and 1985, (b) between 1995 and 2000 and (c) when coupled to a high resolution atmospheric model.

Each of these features warrants further study, but in the rest of this paper the focus is on the the strongest El Niño events when temperatures of 29°C and more are found all across the ocean. In a normal year, as illustrated in Figs. 3 and 4, the average temperatures in the Equatorial Waveguide, between 220°E and 240°E, lie between 24°C and 27.5°C. As shown in Fig. 1, warmer temperatures are found at 8°N, but on average these lie below 28°C and there is not enough heat available locally to explain the warming of the whole of the Eastern Pacific.

4   Zonal advection of warm water near the Equator

In an attempt to clarify how heat was advected in the Equatorial Pacific, the integrated flux of water across a series of longitudes was calculated, with the constraint that the temperature had to be greater than an given minimum value. Figure 5 shows the results plotted as a time series at longitudes 180°E, 210°E and 240°E, for a minimum temperature of 28°C and, at longitude 180°E, for a minimum temperature of 29°C. The figure also includes a series of boxes, covering time periods and latitude ranges of interest, the total flux in each period being summarised in Table 1.
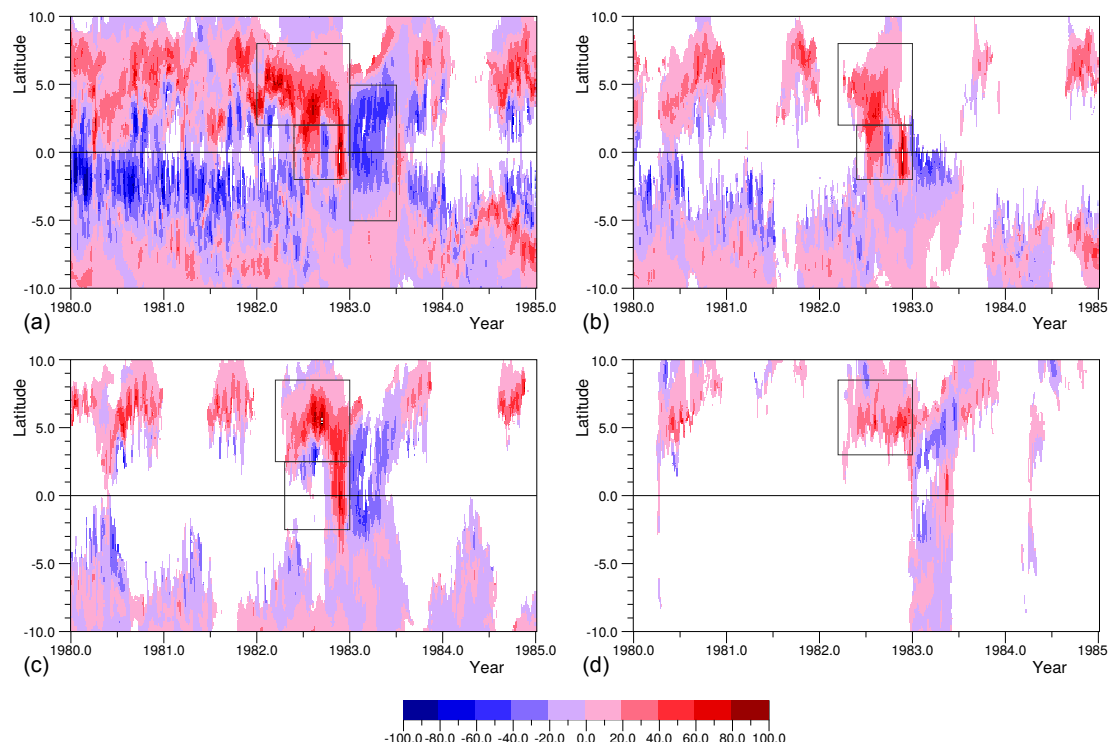
Figure 5. Vertically integrated flux of water ($\mathrm{m^2 s^{-1}}$) with temperature (a) greater than 28°C crossing longitude 180°E, (b) greater than 29°C crossing 180°E, (c) greater than 28°C crossing 210°E, (d) greater than 28°C crossing 240°E. The figure is blank where the flux is zero. Rectangles enclose the regions of table 1.

The figure shows that most of the eastward flow of warm water occurs at the latitudes of the North Equatorial Counter Current. The fluxes are largest in the Autumn of each year, the temperatures in the Spring occasionally being below the minimum temperature. The largest transports occur during 1982, in the period when the 1982-83 El Niño is developing. Thus Figs. 5a and 5b shows stronger than normal flows of 28+°C water at 180°E over most of 1982, and of 29+°C in late summer. At 210°E and 240°E the flow starts later in 1982 and continues until the year end.

In the equatorial band there are long periods when the water at all depths is too cool to contribute to the flux calculations. Longitude 180°E is an exception for a minimum temperature of 28°C, but the flow is predominantly westwards, as is expected for the latitudes of the Equatorial Current. At 180°E and 210°E, large eastward fluxes are observed during 1982, a small event occurring in late summer and a major event just before the end of the year. The major event is also seen at 210°E but is missing at 240°E. However it does show up when the minimum temperature is reduced to 26°C.

South of the Equator an eastward transport of warm water is also seen at the latitudes of the South Equatorial Counter Current. This is unexpected as, east of 180°E, the westward flowing South Equatorial Current is usually thought to be contiguous

Region	Longitude	Minimum Temperature	Southern Boundary	Northern Boundary	Start Year	End Year	Net Flux 10^{12}m^3	Longitude Span
A	180°E	28°C	2.0°N	8.0°N	1982.2	1983.0	484	39.2
B			2.0°S	2.0°N	1982.4	1983.0	124	10.0
C			5.0°S	5.0°N	1983.0	1983.5	-417	-33.8
D	180°E	29°C	2.0°N	8.0°N	1982.2	1983.0	217	17.6
E			2.0°S	2.0°N	1982.3	1983.0	119	9.6
F	210°E	28°C	2.5°N	8.5°N	1982.2	1983.0	310	25.1
G			2.5°S	2.5°N	1982.3	1983.0	79	6.4
H	240°E	28°C	2.0°N	8.0°N	1982.2	1983.0	168	13.6

Table 1. Volume transports of water for the longitudes, temperature classes, latitude bands and time periods denoted in Fig 5. The net flux is given both in units of $10^{12}\,\text{m}^3$ and in terms of the number of degrees longitude that would be covered by the same volume if it was in a layer 100 m thick which extended from 5°S to 5°N.

with the westward flowing Equatorial Current. However the flow is weak and reversing, and does not appear to be connected with the 1982-83 El Niño, so it is not considered further here.

Table 1 shows that at 210°E, the NECC transports a total of $310 \times 10^{12}\,\text{m}^3$ of water warmer than 28°C between the Spring and end of 1982. To give an idea of the potential impact of this volume of water, the table also shows the corresponding span
5 of longitude that it would cover if it was contained in a surface layer 100 m thick extending from 5°S to 5°N.

The table also includes the contribution of the Equatorial band for the same longitude and over roughly the same time period. Although the El Niño is often described as resulting from increased eastward heat advection in the Equatorial Waveguide, the contribution of the NECC is seen to be roughly four times larger than the contribution from currents close to the Equator. This is also true for water warmer than 28°C at 180°E.

10 In each of the three longitudes shown, the flux of water warmer than 28°C is not enough for a layer 100(m) thick to extend from 5°S to 5°N and all the way to South America (at 270°E), but it is sufficient to have a significant impact.

In summary, prior to the peak of the 1982-83 El Niño, sufficient warm water was advected by the North Equatorial Counter Current and the reversed Equatorial Current to produce significant warming of the Eastern Equatorial Pacific. Although it was not possible to to provide a full heat budget[1] there appears to be no reason to look for any other mechanism advocating warm
15 nutrient poor waters into the Eastern Equatorial Pacific prior to an El Niño event.

Whereas most discussions of the El Niño focus on the role of the Equatorial Waveguide, these results show that, in the model, strong Eastern Pacific El Niño events, like the 1982-83 El Niño, occur primarily as a result of heat transported by the North Equatorial Counter Current. Given the good agreement between the model and observations, discussed earlier, this is also likely to be true for the real ocean.

---

[1]This is because of problems in reproducing the model mixing using only the data available in the 5-day average data sets.
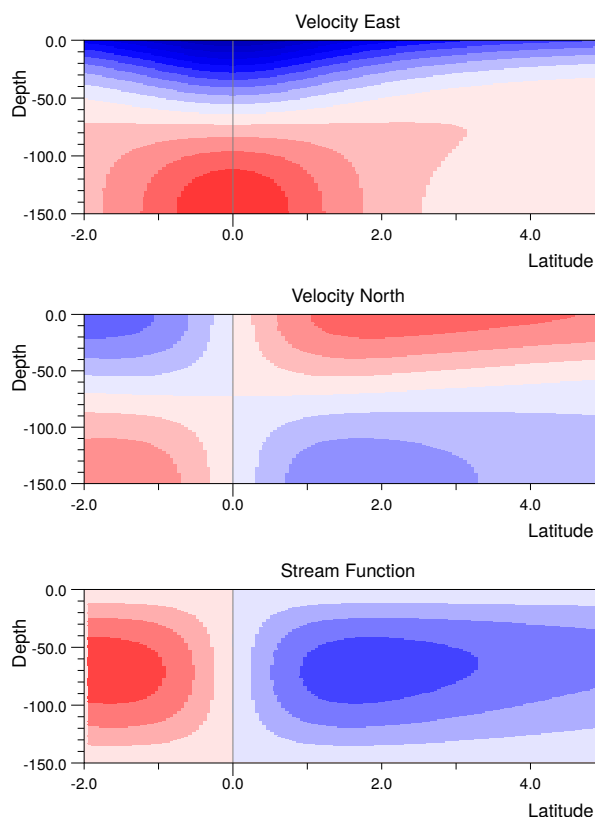
Figure 6. Solution of Stommel's model of the tropical cell, for a surface layer 150 m deep, of constant density and with a vertical kinematic viscosity of $100\,\mathrm{cm^2s^{-1}}$. Velocity contours at intervals of $5\,\mathrm{cm\,s^{-1}}$. Positive values in red.

5 Heat transport and the NECC

These results raise the question of why the NECC might transport so much heat in an El Niño year? Alternatively because, as Wyrtki (1975) pointed out, the NECC has its source in the West Pacific Warm Pool, the real question is "Why does the NECC transport so little heat in a non-El Niño year?".

5   Here it is argued that the transport is reduced by the combined effect of the Ekman transport, the geostrophic inflow, both parts of the tropical cell, and tropical instability waves. All of these processes have the ability to remove warm water from the core of the NECC and to replace it by cooler water from the north or south.

Unfortunately our theoretical understanding of these three components and the NECC itself is poor. As a result the argument made here has to be based on a mixture of theory and analysis of the model results.

5.1 The Tropical Cell

This is probably the best understood of the three processes. As discussed by Stommel (1960), an easterly wind at the Equator initially raises the sea level along the western boundary of the ocean. This results in the development of a pressure gradient along the Equator which eventually exactly balances the surface wind stress.

If τ is the wind stress, p the pressure in the ocean, x the distance east and z the depth, then this balance is given by,

$$\tau \quad = \quad \int dz \, \partial p / \partial x. \tag{1}$$

This pressure gradient also affects the upper layers of the ocean north and south of the equator, where it results in a geostrophic flow v_g towards the Equator,

$$\rho f \int dz \, v_g \quad = \quad \int dz \, \partial p / \partial x,$$
$$= \quad \tau, \tag{2}$$

where ρ is density and f the Coriolis term.

As the east-west pressure gradient changes only slowly with latitude, close to the Equator it can be considered as a constant, which means that the integral of v_g tends to plus or minus infinity as $1/f$ as the Equator is approached.

Away from the Equator the surface wind stress generates an Ekman transport, v_e, such that,

$$-\rho f \int dz \, v_e \quad = \quad \tau. \tag{3}$$

This integral also tends to plus or minus infinity as the equator is approached. However the singularity in v_e exactly balances that in v_g, so as shown in Fig. 6, overall the solution is well behaved. In fact it is so well behaved that as well as the Ekman transport away from the Equator and the geostrophic inflow towards the Equator, the solution also includes the Equatorial Current and the Equatorial Undercurrent.

Unfortunately the theory has a major flaw. Stommel (1960) treated the ocean surface layer as one of constant density and with a constant vertical viscosity. He then found that if the vertical viscosity was reduced enough to generate a realistic undercurrent speed then the width of the undercurrent was only a fraction of a degree, whereas in reality it is a few degrees wide. If the viscosity is increased by a factor of 10, as it has been for Fig 6, then a reasonable width can be obtained but the maximum undercurrent velocity is only $25 \, \mathrm{cm \, s^{-1}}$ instead of a more realistic $150 \, \mathrm{cm \, s^{-1}}$.

The solution to the problem was eventually found by McCreary (1981) who showed that it was necessary to introduce stratification. When this was modeled semi-analytically, the upwelling near the equator was limited by the rate at which heat could diffuse downwards. This has a number of effects. First it increases the range of latitudes over which upwelling occurs. Secondly the Ekman transport reduces sea level near the Equator and results in a compensating raising of the density surfaces below. This in turn increases the temperature gradient and aids the downward diffusion of heat.

The main point though is that near the Equator the poleward Ekman transport due to the wind is balanced by a shallow geostrophic inflow. This can be seen in Fig. 2, where at 6°N the Ekman transport has speeds of order $5 \, \mathrm{cm \, s^{-1}}$ and above 150 m the geostrophic inflow has speeds of around $1 \, \mathrm{cm \, s^{-1}}$. At the same longitude the core of the NECC lies in the top 150 m,
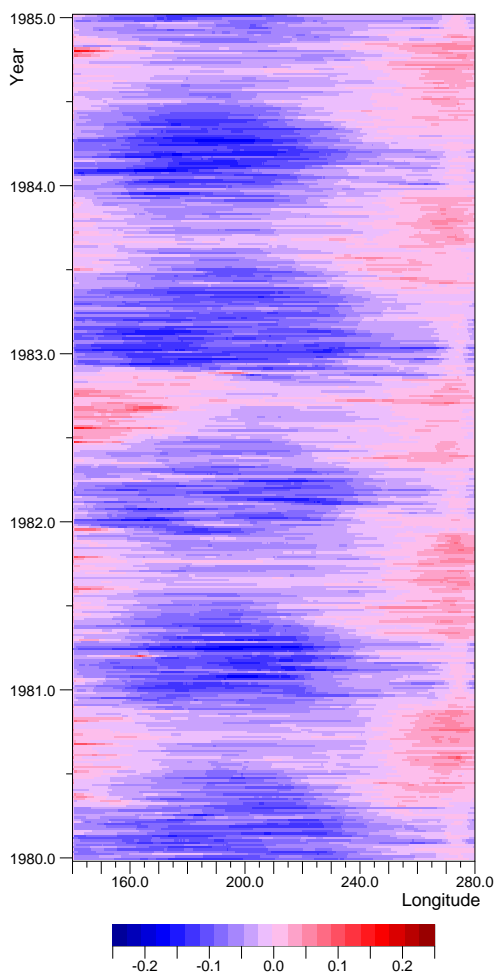
Figure 7. Eastward component of wind stress (Pa) at 6°N in the Equatorial Pacific between 140°E and 280°E (80°W), between 1980 and 1985.

with speeds of only 20-30 $\mathrm{cm\,s^{-1}}$. As a result, given the size of the Pacific Ocean, even small secondary flows can have a significant influence on the core waters transported by the NECC.

5.1.1 Ekman transport

Figure 7 shows the eastward component of wind stress at 6°N plotted as a function of longitude and time. It shows a regular
5 pattern each year, the wind stress in the Central Pacific being largest during the Northern Spring and weakest in Summer. The
year 1982 is unusual as the stress drops to near zero near the dateline for a large part of the Summer and Autumn. This is show
more clearly in figure 8.
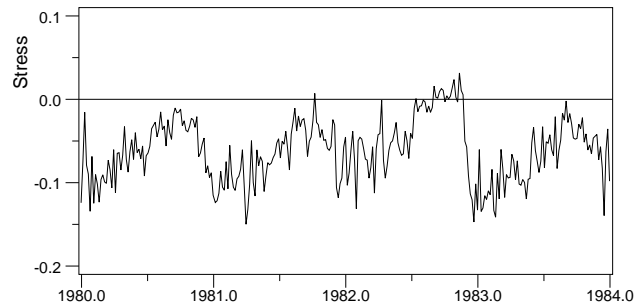
Figure 8. Eastward component of wind stress (Pa) at (180°E, 6°N) between 1980 and 1984.

At 6°N, the Coriolis term equals 1.52×10^{-5} s^{-1}, so if the water density is taken as 1024 kg m^{-3}, then from Eq.3, the northward transport due to a westward wind stress of 1 Pa is 64.2 m^{2}s^{-1}. From Figs. 7 and 8, the westward stress in mid ocean lies around 0.1 Pa in Spring dropping to half that value in the Autumn. A value of 0.05 Pa will generate a northward Ekman transports 3.2 m^{2}s^{-1}, equivalent to 0.36 Sv per degree of longitude. This appears small compared to the NECC transport but

5 over longitude span of twenty to thirty degrees or more it will become significant.

Figure 7 shows that in the Autumn of 1982 the zonal wind stress was small over much of the Central Pacific. During this period the Ekman transport would have been much less effective in cooling the warm core of the NECC. The figure also shows that the reduction in Central Pacific winds at this time correlates well with the arrival of warm water shown in figure 4.

5.2 Geostrophic inflow

10 The meridional component of geostrophic transport V_g, is related to the zonal gradient of P and the vertical integral of the pressure p, by the equations,

$$
\begin{aligned}
V_g &= (1/(\rho f)) \; \partial P/\partial x, \\
P &= \int_{-300}^{z_{ssh}} dz \; p(z).
\end{aligned}
\tag{4}
$$

where z_{ssh} is the sea surface, z is depth and x is the co-ordinate in the zonal direction. The lower limit of 300 m was chosen

15 because the horizontal gradient of pressure is small at greater depths and the limit is below the normal depth of the NECC.

In Figs. 9 and 10, these variables are plotted as functions of longitude and time for a latitude of 6°N. As expected, the integrated pressure field is usually greater in the west than in the east, a typical mean gradient between 260°E and 170°E being 0.035 Pa m^{-1}. This corresponds to a southward transport of 2.2 m^{2}s^{-1} or 0.25 Sv per degree of longitude over the whole Pacific. As might be expected (Fig. 7) this is less than northward Ekman transport near (180°E, 6°N) based on the local winds.

20 A second feature that might have been expected near 6°N is the annual wave (Myers, 1979) which shows up in the integrated pressure field. This has a minimum which starts at the eastern boundary each Northern Winter and which reaches the Western
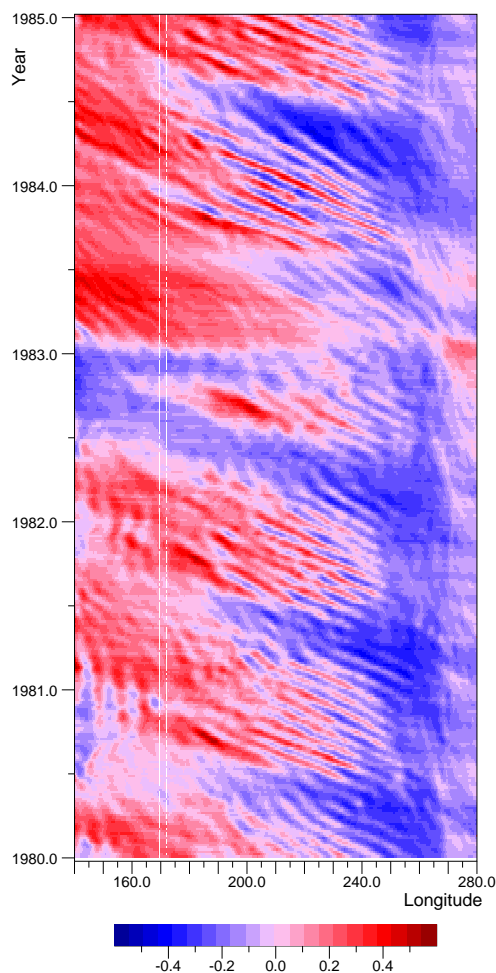
Figure 9. Pressure integral (10^6 Pa m) of Eq. 4 at 6°N and at 300 m (after subtracting constant equal to integral with density of 1024 kg m^{-3} and zero surface elevation). Vertical lines are due to shallow topography.

Pacific in the following Autumn. In most years the wave tends to die out west of 200°E, but in 1982 during the development of the El Niño, this does not happen.

In this year there is also a lowering of sea level close to the western boundary, similar to an event seen in 1980. Towards the end of the year there is a rapid reduction in sea level which affects the Western and Central Pacific.

5   The waves are significant in that they are large enough to reduce and change the sign of the east-west pressure gradient. Thus, and especially in 1982, they can significantly affect the flushing of the NECC by the geostrophic inflow.
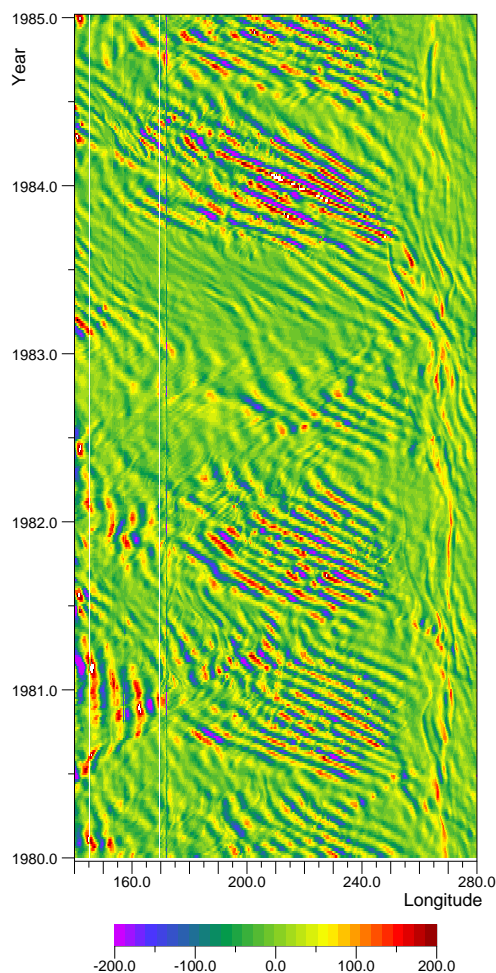
Figure 10. Northward component of geostrophic transport ($\mathrm{m}^2\mathrm{s}^{-1}$), defined by Eq. 4, at 6°N.

As in Fig. 4, Figs. 9 and 10 show short wave features which appear to be the result of tropical instability waves. Fig. 10 shows that the meridional transport due to the features can reach values of over 20 $\mathrm{m}^2\mathrm{s}^{-1}$ or 5.6 Sv/degree, sufficient to dominate the transport of the NECC. This aspect is discussed further in the following section.

5.3 Tropical instability waves

5   Tropical instability waves are wave motions observed north and south of the Equator in the Pacific and Atlantic Oceans. They show up most clearly in the surface temperature field as fronts between the cooler equatorial waters and warmer waters to the north and south. In the Pacific they are most noticeable in the Eastern Pacific in the late Northern Summer and Autumn.
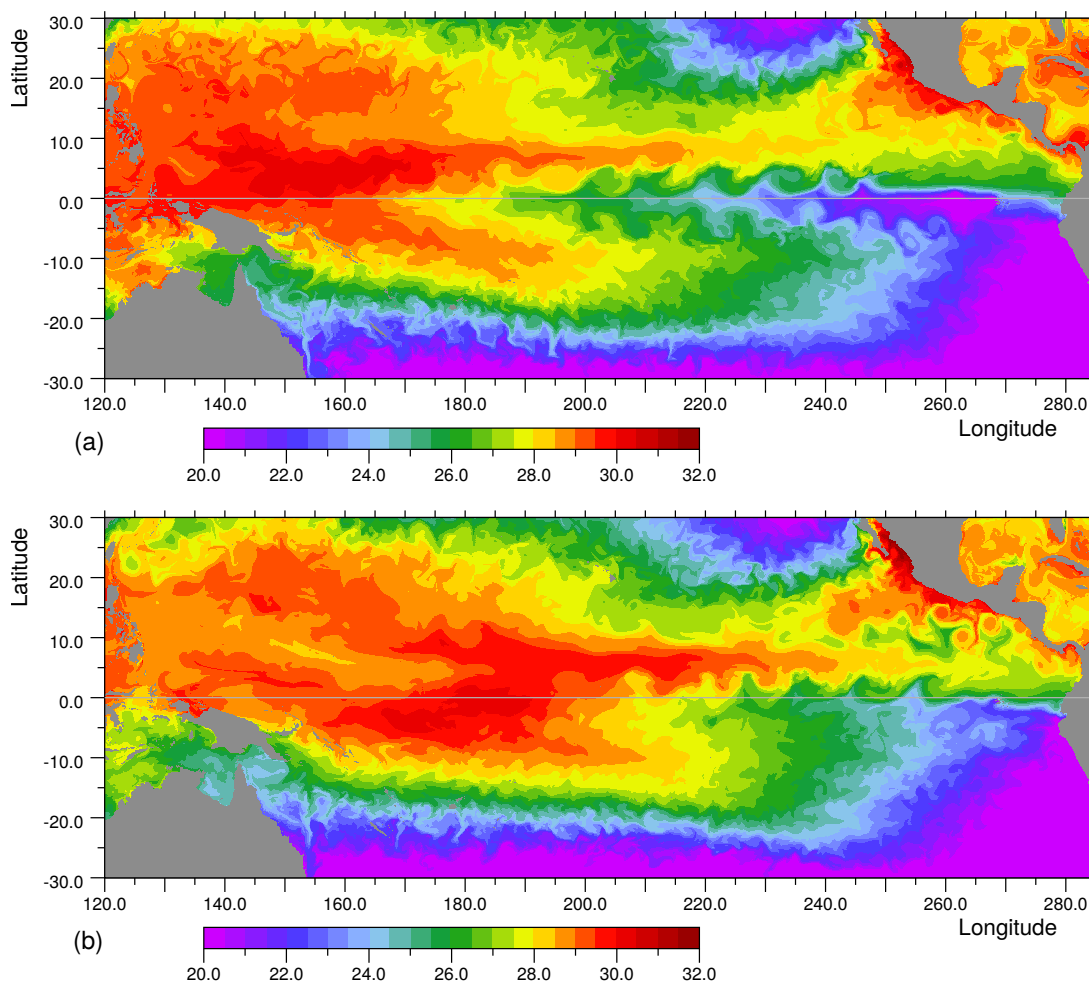
Figure 11. Surface temperature (°C) from the model in late September (a) 1981 and (b) 1982. (Values below 20.5°C combined).

Understanding of the waves has come primarily through numerical model studies. Philander (1978) used a two layer model and showed that the waves growth was due primarily to a barotropic instability resulting from the strong shear between the Equatorial Current and the North Equatorial Counter Current. Cox (1980), using a multi-layer model, confirmed the importance of barotropic instability but also found that baroclinic instability was involved when the amplitude became large.

5   However this picture was not supported by the study of Luther and Johnson (1990). They analysed observations made during the Hawaii-to-Tahiti shuttle experiment and found that the main instability lay just south of the Equator and was due to the shear between the Equatorial Undercurrent and the South Equatorial Current. Also unlike Philander and Cox they found an instability between the Equatorial Current and the NECC in the northern winter and a baroclinic instability of th NECC during the Northern Spring.

These inconsistencies have never been properly explained, but later studies both observational and numerical (Menkes et al., 2006, see the Menkes paper for more references) support the earlier analysis of Philander and Cox.

Figure 11 shows the model surface temperature fields for late September in 1981 and 1982. The first shows a series of well developed of Tropical Equatorial Waves just north of the Equator starting near 250°E and extending west to beyond 210°E. The corresponding velocity field shows a series of oval anti-cyclonic eddies with an west-east width of about 10 degrees with southern and northern limits at approximately 1.5°N the 7.5°N. The eddies tend to be confined to the top 300 m, the 28°C isotherm which is at a depth of ~ 20 m at the equator dropping to around 200 m in the centre of each eddy. Below 200 m the eddy signature drops off rapidly, so although there is some displacement of the isotherms near 500 m the isotherm displacements are very small below that depth.

The eddies are affected by the tropical cell. As a result at a depth of 30 m, maximum northward velocities near 5 °N, are $\sim 1 \, \mathrm{ms^{-1}}$ and maximum southward velocities $\sim 0.6 \, \mathrm{ms^{-1}}$. In contrast at 108 m, maximum northward velocities are $\sim 0.85 \, \mathrm{ms^{-1}}$ and maximum southward velocities $\sim 1 \, \mathrm{ms^{-1}}$.

5.3.1 TIW variability

Given the potential impact of tropical instability waves on the NECC it is useful to have a measure of how their impact may change with time. This may be achieved by first estimating V_{300}, the northward transport in the top 300 m of the ocean,

$$V_{300} = \int dz \, v. \tag{5}$$

This is then smoothed in space to give $\bar{V}$ and the r.m.s. variance defined as,

$$\bar{V} = H(V_{300}),$$
$$V_{rms} = H(|(V_{300} - \bar{V})|). \tag{6}$$

where $H()$ is a Hann filter with a width of 20°of longitude.

The result at 6°N is shown in Fig 12. In most years the r.m.s. transport after smoothing has values around $30 \, \mathrm{m^2 s^{-1}}$, consistent with the peak values discussed previously. However what is very significant is the region of very low variability that starts in the west, in mid 1982 and which moves across the Pacific during the latter part of the year. The variability then stays low for a large fraction of 1983.

As the generation of TIWs is partly associated with the Equatorial Current, it is possible that the low variability results from reduction in the Equatorial Current as the El Niño develops and the low wind stress region moves east.

Figure 13 plots the strength of the surface Equatorial Current as a function of longitude. The region of reduced activity of Tropical Instability waves, seen in 1982, fits very closely with the region of reduced and reversed currents at the Equator.

This feature can also be seen in Fig. 11 where in September 1981, tropical instability waves are mixing cooler equatorial waters into the NECC between 180°E and 200°E. In September 1982 these are not present and the warm core of the NECC is advected much further east before such mixing events occur.
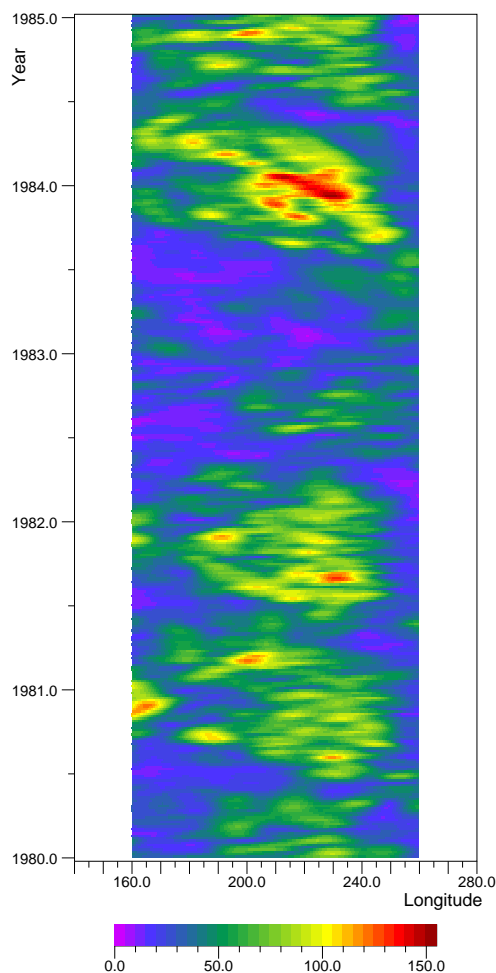
Figure 12. The r.m.s. northward transport variability V_{rms} (defined in Eq. 6) along latitude 6°N. Units of $\mathrm{m^2 s^{-1}}$

5.4 The North Equatorial Counter Current

Any attempt to define the strength of the eastward flowing NECC is complicated by the fact that near the Equator it is often connected to the eastward flowing Equatorial Undercurrent and that at times the wind driven current at the equator may reverse direction. For that reason it is convenient to define the NECC as the region of eastward velocities lying between 3°N and 8°N where, at the same location, the surface velocity is also positive.

Figure 14, plots the transport defined in this way, but extending to the equator for a longitude of 180°E. It illustrates the large variability in the current in most years. Examination of the surrounding velocity field when the transport drops or is missing has shown that it is primarily due to oceanic eddies. The large values seen near the Equator arise from the reversal of the surface current at the Equator together with the contribution from the Equatorial Undercurrent.
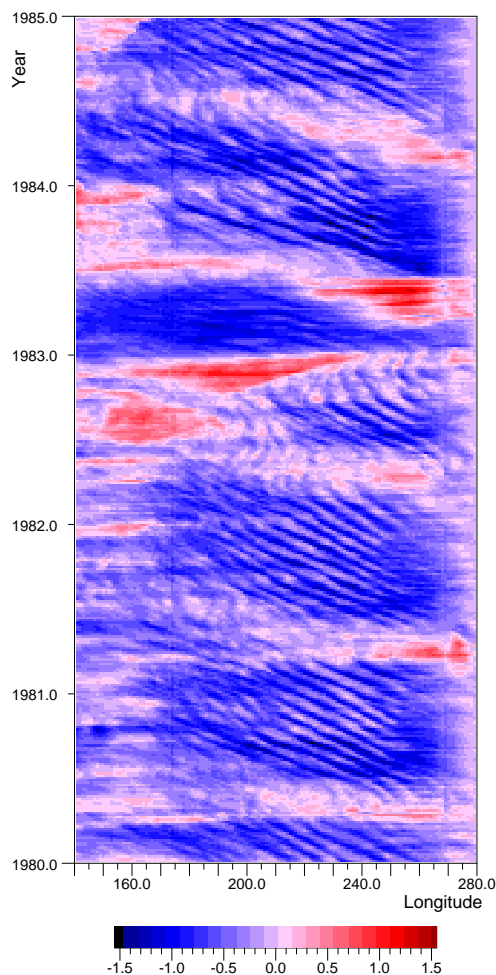
Figure 13. The surface current on the Equator $(\mathrm{m\,s^{-1}})$, averaged between 1°S and 1°N, plotted as a function of longitude and time. Negative values correspond to the normal westward flowing Equatorial Current.

The year 1982 is seen to be very unusual. First the current is continuous, consistent with the reduction in current variability discussed previously. Secondly the peak and average transport in the current appears to increase with the peak value reaching $140\,\mathrm{m^2 s^{-1}}$. Thirdly the latitude of the current core appears to move southward, lying near 5 °N rather than the 7°N that predominates in 1981 and 1982.

5   Figure 15 plots the total transport between 3°N and 8°N. This shows that the total transport of the NECC averages between 15 and 20 Sv but in 1982 it doubles to between 30 and 40 Sv.
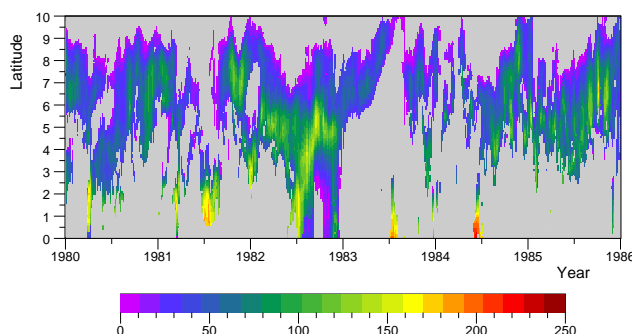
Figure 14. Eastward transport $(\mathrm{m^2 s^{-1}})$ of the NECC across 180°E, plotted as a function of latitude and time. The transport here is defined as the integral of the eastward component of velocity from the surface to the first level where it is negative. It is zero if the surface velocity is westward.
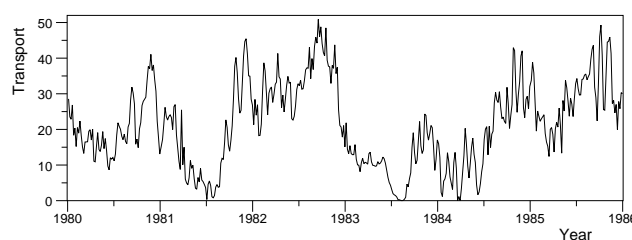
Figure 15. Total transport (Sv) between 3°N and 8°N of the NECC across 180°E.

6   Differences in El Niño years

The results presented so far show that the NECC can at times transport large amounts of warm water into the Eastern Pacific and so trigger an El Nino. They also shown that in most years this does not happen because tropical instability waves, the Ekman transport and the geostrophic inflow combine to dilute the warm core of the NECC with cooler water from the north

5   and south.

However in an El Niño year, once the main atmospheric convection region and the associated region of low wind stress, have started moving eastwards, the strength of these processes is reduced in the ocean to the west. As a result the core of the NECC reaching the convection region is much warmer than normal for those longitudes and as it continues eastwards it has the potential to trigger further convection, thus moving the region of atmospheric convection steadily eastwards.

10   This poses the question "Why does an El Niño occur every year?", or given that the processes that start an El Niño has not been discussed "Why is not every El Niño a strong El Niño like the one in 1982-83?".
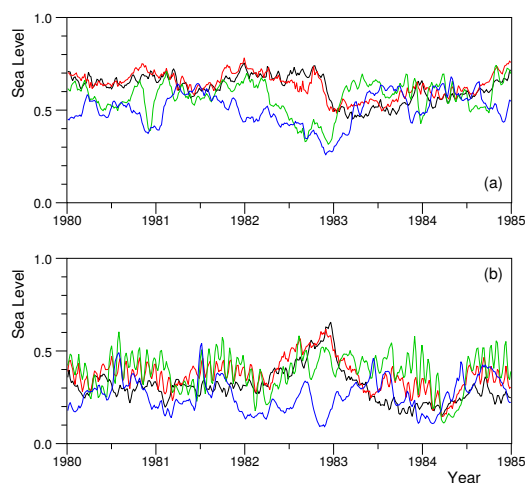
Figure 16. Sea surface height (m) at longitudes: (a) 168°E, (b) 230°E and latitudes: (black) the equator, (red) 3°N and (green) 6°N and (blue) 9°N.

One possibility, originally proposed by Wyrtki (1974) and supported by the results of the last section, is that the year to year differences are, in part, a result of changes in the strength of the NECC. For this reason the next sections consider the year to year differences in more detail.

6.1 Wyrtki's NECC estimate based on sea levels

5 Wyrtki (1974) estimated changes in the strength of the NECC from sea level measurements made at Kiritimati (Christmas Island, 01°52'N 157°24'W) on the Equatorial Ridge and Kwajalein Atoll (8°43'N 167°44'E) on the Counter Current Trough. He found that the height difference was largest, and the NECC presumably strongest during the El Niños of 1957-58, 1963-64 and 1967-68.

The model data was analysed in the same way and it was found that the SSH difference between 3°N and 9°N correlated
10 with the average surface currents between those latitudes. In particular they both showed significant increases during the same periods in the autumns of 1982 and 1997, when the strong El Niños shown in Fig. 3 were developing.

Wyrtki's analysis showed that the change in NECC strength was due primarily to the lowering of SSH in the trough. As shown in Fig. 16a, at 168°E, the longitude of Kiritimati, the models results agree with this. They show a reduced sea level in the trough (9°N) during the latter half of 1982 but a roughly constant sea level near the equator during the same time period. At
15 other times, sea level at 3°N is usually slightly above that at the Equator, a result of the Equatorial Trough that develops when the westward flowing Equatorial Current is present.

Further east at 230°E (130°W) (Fig. 16b) the behaviour is very different. Sea level differences between latitudes are generally smaller and there is a strong annual signal, especially at 6°N. Again there is a large sea level difference between the equator and 9°N in the autumn of 1982 but here it is also due to an increase in sea level at the Equator.
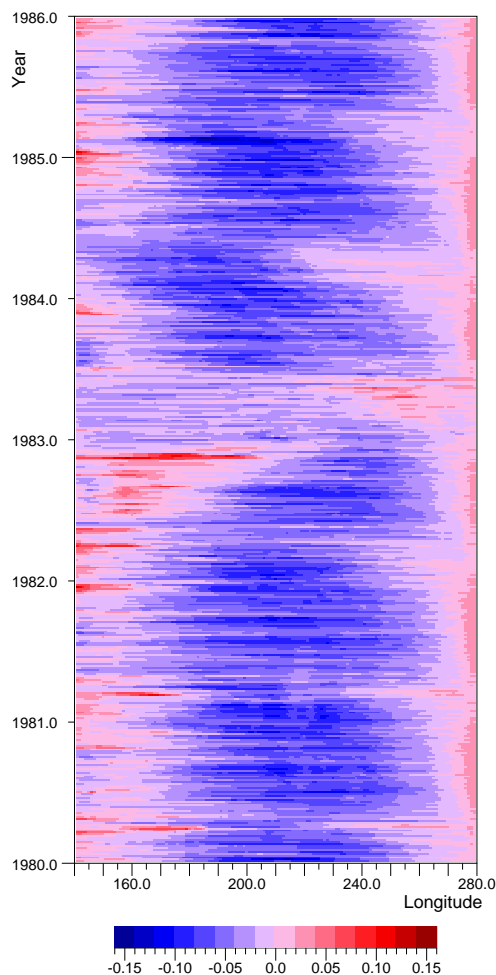
Figure 17. Eastward component of wind stress (Pa) at the Equator between 140°E and 280°E (80°W).

Thus the model agrees with Wyrtki's result for Kiritimati but it also indicates that the full picture is much more complex. To understand more it is convenient to investigate the changes in sea level with both longitude and time at each latitude.

6.2 The annual wave and other processes

Figures 18 to 20 show the sea level plotted as a function of longitude and time at the Equator, at 3°N, at 6°N and at 9°N.

5   Starting with the equator, the figure shows that, except during the 1982-83 El Nino event the east-west slope remains relatively constant. Eastward traveling Kelvin waves occur at regular intervals, producing an increase in sea level which returns to normal after the wave has passed.

In this figure the El Nino event starts in the middle of 1982 when the sea level in the west drops and the region of maximum sea level moves to approximately 190°E. The initial movement may be associated with a Kelvin wave, but the maximum then
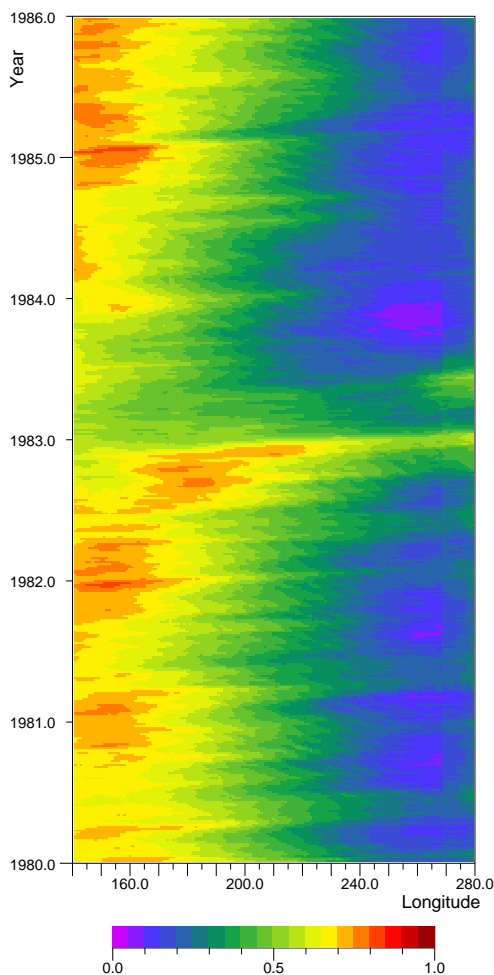
Figure 18. The model SSH (m) at the Equator as a function of time and longitude.

remains fixed, despite further Kelvin waves, until near the end of 1982 when sea level drops rapidly all along the equator. This collapse is certainly associated with a Kelvin wave.

Following the collapse, sea level stays low throughout 1983, recovers slightly in 1984 and only returns to normal at the start of 1985.

5   At 9°N, sea level again shows a mean east-west slope, but at large scales it is highly variables, the east-west differences being largest in the middle of 1981, 1983 and 1984 and smallest at the end of 1982. The latter occurring around the period when sea level dropped along the Equator. However, unlike the Equator, sea level rapidly recovers in 1983 to a value in the west even higher than in 1981.
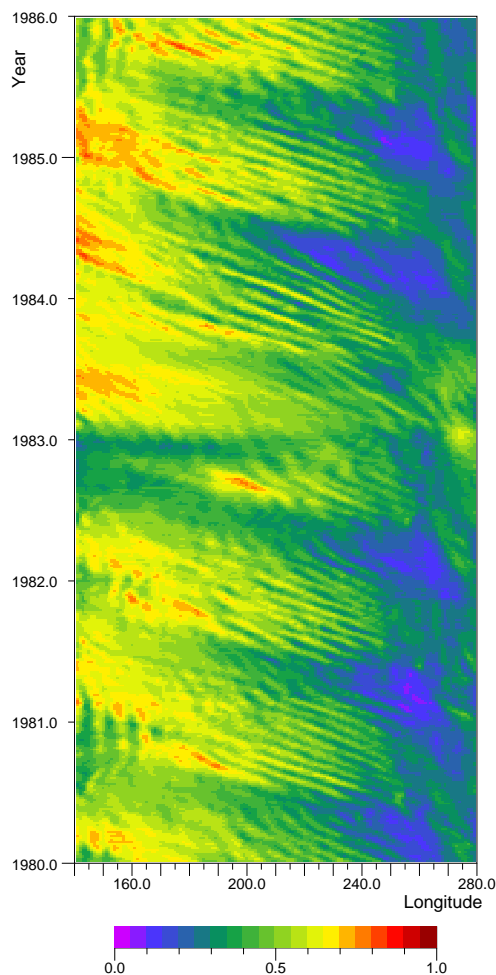
Figure 19. The model SSH (m) at 6°N as a function of time and longitude.

Sea level at 9°N also shows short period and short wavelength Rossby wave like features moving westward at all times. The features may be partly due to Tropical Instability waves, but the region is also affected by eddies along the edge of the North Equatorial Current.

The annual signal at 9°N is strong and to first order appears to consist of two main components. The first is a change

5 independent of longitude which has its maximum in the middle of each year. The second is a set of westward traveling waves, an example of which is the minimum in sea level that starts at the eastern boundary in the autumn of 1981 and which reaches 200°E at the end of 1982.

At 6°N, sea level also shows an annual variation, but here the signal appears to be dominated by a westward traveling wave. Like the wave at 9°N this starts at the eastern boundary each autumn. In reaching 260°E (100°W), the approximate longitude
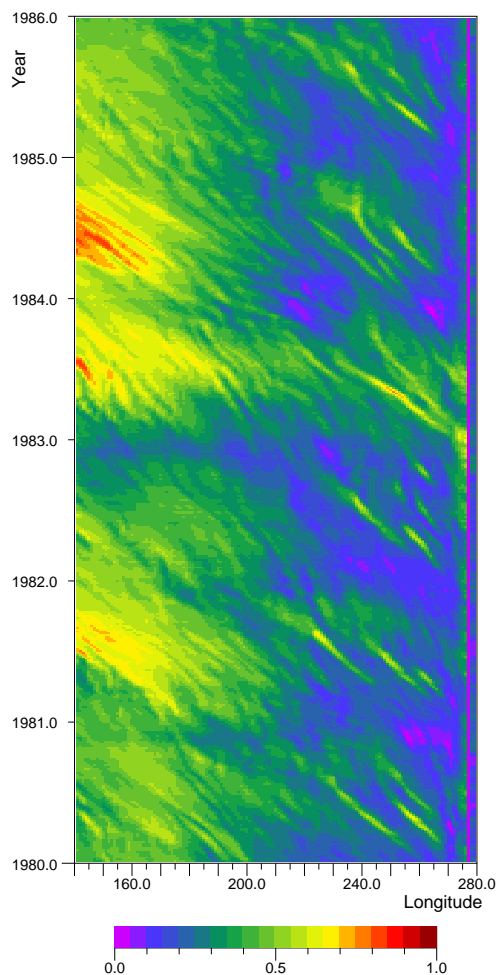
Figure 20. The model SSH (m) at 9°N as a function of time and longitude.

of the Galapagos Islands, in the northern spring where it is associated with a minimum in sea level. It then moves westward more rapidly, the leading edge reaching the western boundary in mid year and the trailing edge arriving before the end the year.

The propagation of the 1982 minimum in sea level at 6°N appears to be unusual in that at 230°E minimum is similar to the value in 1981 but in the region west of 180°E the minimum is much lower.

5   As shown in Fig. 16, at 168°E the passage of the wave results in the sea level at 6°N being similar to that at 9°N at a time when sea level at the Equator remains high. Thus although the meridional pressure difference across the NECC remains roughly constant, the current is squeezed into a path nearer the Equator, where the Coriolis term is smaller. As the current is in geostrophic balance, its transport must increase.

Thus in principal the passage of a stronger than normal annual wave can increase both the strength of the NECC and its heat transport, and so be more effective at moving the centre of atmospheric convection further east.
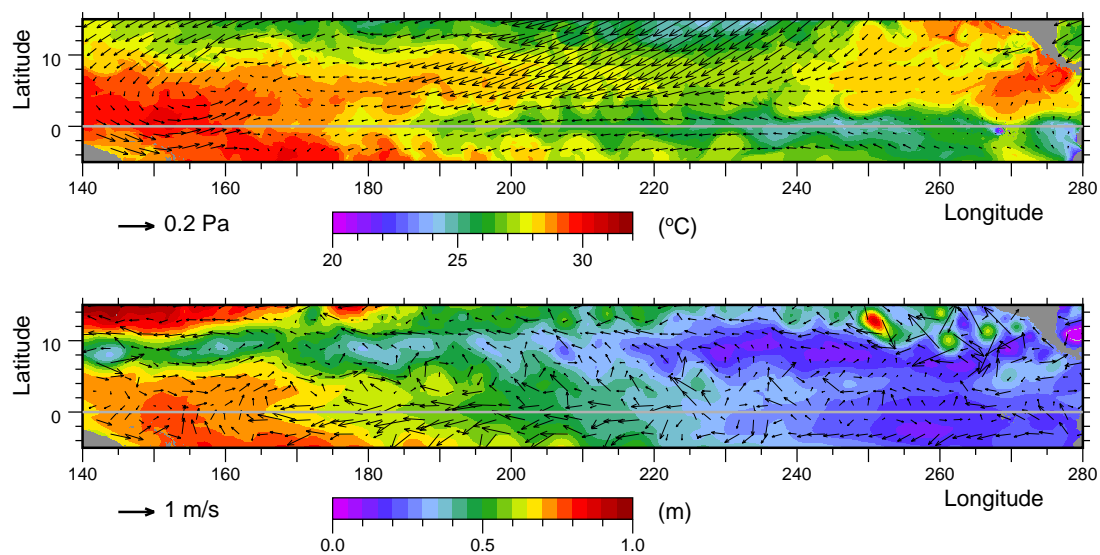
Figure 21. Upper: Surface temperature and wind stress vectors. Lower: SSH and velocity vectors from the 30th March 1982 archive dataset. Each archive dataset contains averages over the previous 5 days of the model run.
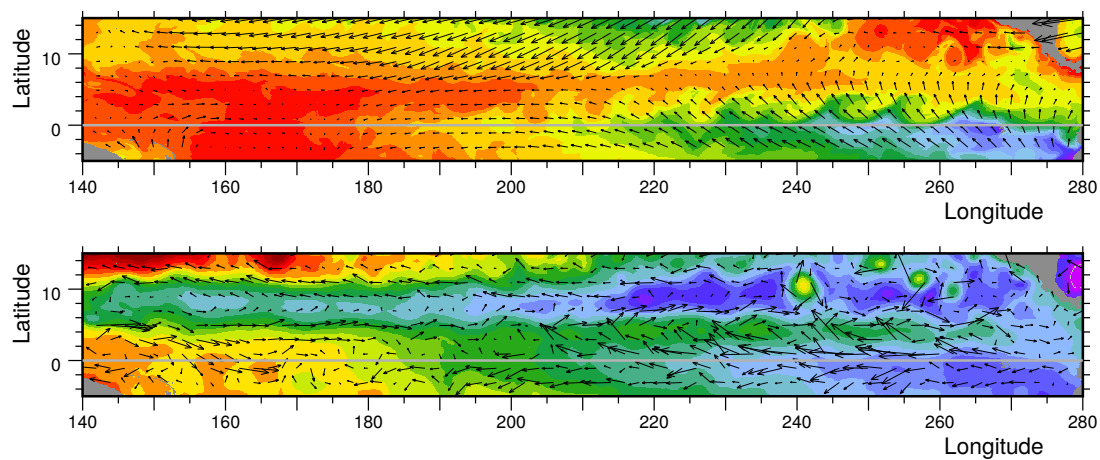
Figure 22. Upper: Surface temperature and wind stress vectors. Lower: SSH and velocity vectors from the 30th June 1982 archive dataset. Colours and vector scales as in Fig. 21.

6.3 Development of the El Nino during 1982

The discussion so far has concentrated on individual physical processes with only limited discussion of the overall development of the El Niño. To give more context, the following sections briefly discuss some of the other events that occurred in the Equatorial Pacific during 1982 and how these may be connected to the processes discussed above.

6.3.1 30th March

Figure 21 shows fields of SSH and surface temperature together with the surface velocity and wind stress vectors for the 30th March 1982. At this time the minimum in the annual wave at both 6°N and 9°N is still in the Eastern Pacific, where it contributes to the minimum in the NECC trough near 240°E. The vector plot shows that he NECC is a weak feature, except between 140°E and 160°E where it runs along the northern flank of a region of maximum SSH.

The figure also shows the Equatorial Current in the Central Pacific with sea level ridges to north and south on which can be seen maxima due to tropical instability waves. The warmest temperatures on the equator are found north-east of new Guinea and this is also the region where the SSH along the Equator is highest.

The figure shows a westerly wind burst, which occurred at the end of March and on this basis it may be tempting to ascribe the position of the SSH maximum to the westerly winds often found in this region. However dynamically the Mindinau and Halmehera Eddies and the two South Pacific inflows, the New Guinea Coastal undercurrent and the New Ireland Current, may also be involved.

6.3.2 30th June

By the end of June the annual wave at 6°has reached the Western Pacific and the wave at 9°N has reached 230°E. As a result the NECC trough is deeper and more uniform throughout the Central and Eastern Pacific. The North Equatorial Ridge in the Western Pacific has also developed, and this, together with the changes in the NECC trough result in a much stronger NECC all across the Pacific.

In the west, SSH on the equator has dropped slightly, but this is the time that in Fig. 18 the maximum SSH is in the process of moving from around 150°E to 190°E (170°W). The region of low winds has started to expand, temperatures have risen, including along the line of the NECC, and the current is more effective at transporting warm water to the east, beyond the region of low winds.

6.3.3 30th September

This lies in the middle of the time period when the maximum SSH along the Equator lies near 190°E. The region of high SSH is also one of increasing temperatures which steadily grows with time on both sides of the Equator. One consequence of this is the region of higher than normal sea level at 20°E, 6°N seen in Fig 19.

By this time the NECC has also grown in strength and in seen to move northwards as it crosses the ocean, starting near 4°N and reaching 8°N near 240°E.
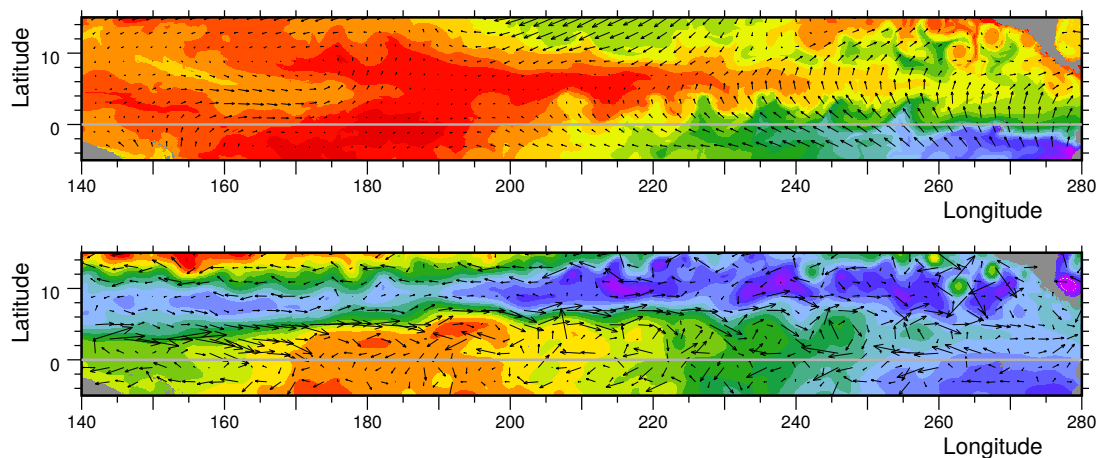
Figure 23. Upper: Surface temperature and wind stress vectors. Lower: SSH and velocity vectors from the 27th September 1982 archive dataset. Colours and vector scales as in Fig. 21.
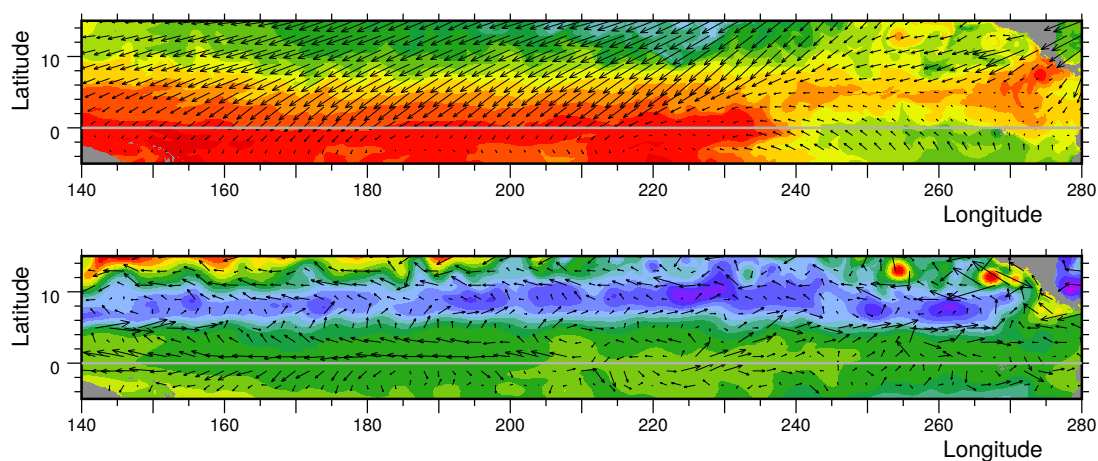
Figure 24. Upper: Surface temperature and wind stress vectors. Lower: SSH and velocity vectors from the 31st December 1982 archive dataset. Colours and vector scales as in Fig. 21.

This is also a this period when westerly wind bursts develop. These can be seen in Fig 17 and the resulting Kelvin waves in Fig 18. However these occur in the region where the mean wind is now westerly and there is no evidence that the resulting eastward surface current along the Equator in this region is significantly different from that to be expected with just the steady westerly wind.
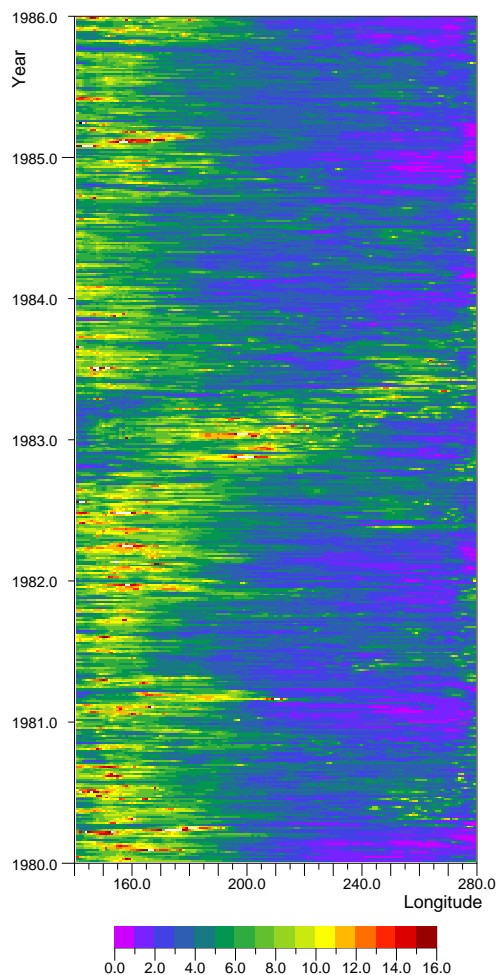
Figure 25. Precipitation $(\mathrm{kg\,m^{-2}d^{-1}})$ averaged between 12°S and 12°N as a function of time and longitude.

6.4 30 December

In October and early November 1982 the Central and Western Equatorial Pacific was a region of light westerly winds interspersed by stronger westerly wind bursts. In contrast in the Eastern Pacific, a strong trade wind continued to blow.

In late November the pattern changes and strong westerly winds blow along the equator on either side of the dateline. These
5 result in an eastward flowing surface current which continues until the end of the year (Fig. 24), advecting the warm water patch on the equator towards the east.

By the end of the year, the trade winds are starting to be reestablished north of the Equator. In the west the westwards flowing Equatorial Current is reforming and by the 10th January it is again established in the east, as a result carrying the patch of warm water back towards the Central and Western Pacific.

However, as shown in Fig. 25, this is the time that precipitation is most established in the Central Pacific. Precipitation remains high in the Central Pacific during the remainder on the Southern Hemisphere summer after which it first moves closer to South America before the high precipitation region is reestablished in the Western Pacific.
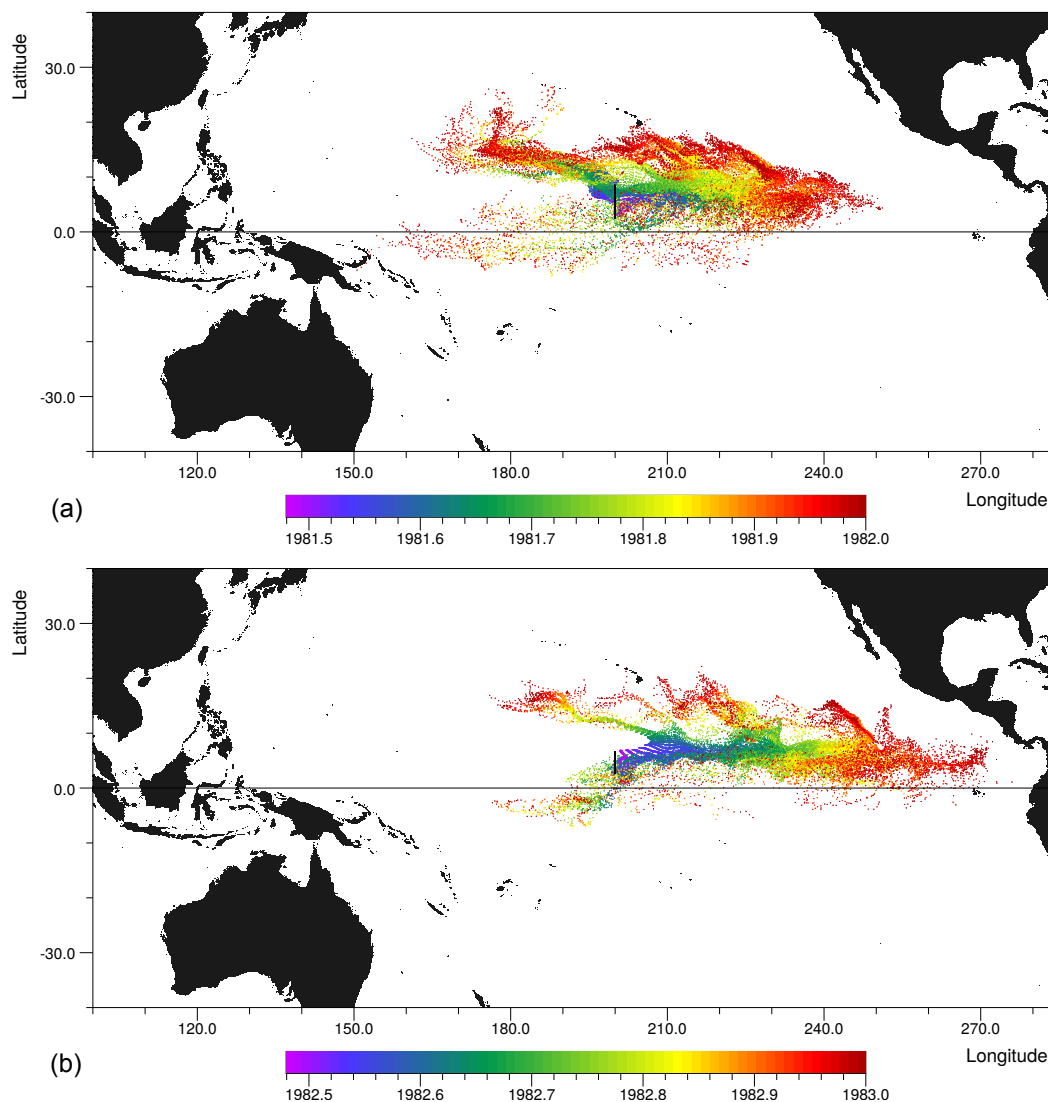
Figure 26. Water particle positions plotted every 5 days, starting from the 24th June (a) 1981 and (b) 1982 and running to the end of the year. The date is denoted by the colour of each dot. For the initial state, one particle was placed at the centre of each model grid cell lying along the black line, having a water temperature of greater than (a) 27.8°C and (b) 29°C, there being no water with a temperature greater than 29°C along the line in 1981.

7 Particle tracking

A useful alternative view of the processes can be obtained using the Tracmass particle tracking program (de Vries and Döös, 2001). Figure 26 shows the results of seeding the NECC at 200°E in June 1981 and 1982. This is the time when in 1982 the NECC was carrying water warmer than 29°C into the Western Pacific.

5   In 1982 each model grid box along the line shown, with a temperature greater than 20°C, was seeded with a single particle. In 1981 there was no water along the line with this temperature so boxes were seeded where the temperature was greater than 27.9°C.

In 1981, the water was initially carried east but before reaching the far Eastern Pacific most particles moved north, where they were carried westward by the North Pacific Sub-tropical Gyre. The remainder moved south and were carried westward by
10   the Equatorial Current.

By contrast, in 1982 the much warmer water was carried predominantly to the east with a significant quantity reaching as far as the Galapagos islands. Particles were carried to the north and south, but fewer were lost in this way than in 1981.

In two other runs (not shown), particles were seeded in the Niño 1 and 2 regions, which are to the south-east of the Galapagos Islands. The tracking program was then run backwards in time, from early in 1982 and 1983, to determine where the water
15   came from.

In 1982 the water was found to have a local origin, some coming from upwelling regions near the coast. In contrast in 1983 a significant amount came from just north of the Galapagos, apparently displaced by the water entering the region shown in Fig. 26. Observations made in 1981 and late 1982 show a similar movement of warm, low nutrient, surface water southwards across the Equator at this time (Barber and Chavez, 1983).

20   In a final test, water particles were tracked moving eastward along the Equator. The model showed that in late October 1982, following the reduction and reversal of the winds, the Equatorial Current at 200°E also reversed direction. The region of water warmer than 29°C, shown in Figs. 11 and 23, then started moving eastwards along the Equator.

This ocean was seeded as before and Fig. 27 shows the initial seeding line and the later particle positions. The particles are seen to move eastward but they do not progress far. By the end of the year none of the particles have passed 240°E and many
25   have turned back westward.

8 Discussion

This paper is the result of a preliminary analysis of archived data from an early run of a high resolution global ocean model. A previous comparison with observations in the Equatorial Pacific indicated that the model behaved well. Unfortunately the model data, which is available as averages made every five model days, contains only a limited amount of information and so
30   is not suitable for a detailed analysis of the fluxes within the model.

Because of this, the results presented here are primarily qualitative. They do however give a consistent picture of the oceanic processes which contributed to the strong El Niño of 1982-83.
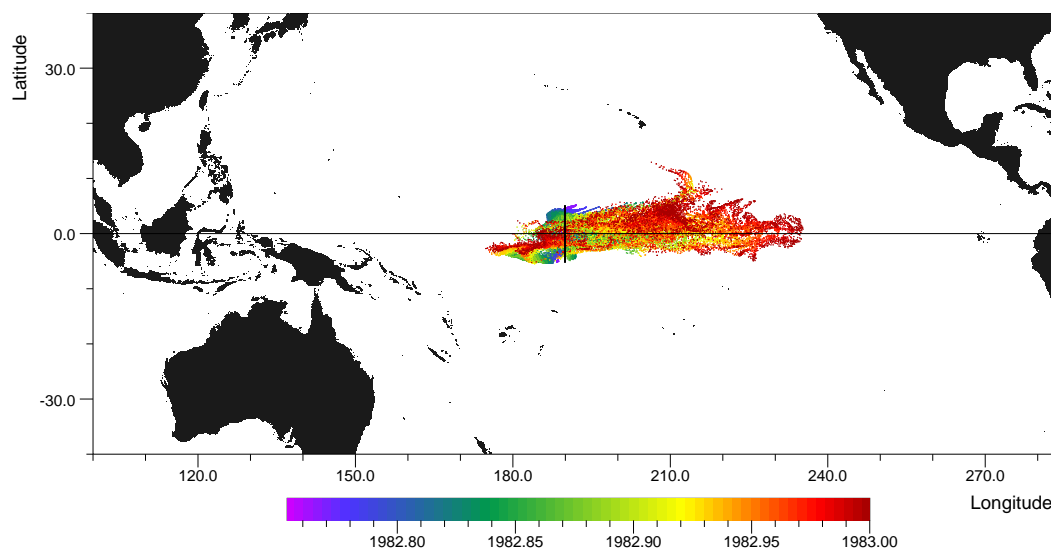
Figure 27. Water particle positions plotted every 5 days between 2nd October 1982 and the end of the year, the date being denoted by the colour of each dots. For the initial state, one particle was placed at the centre of each model grid cell lying along the black line having a water temperature of greater than 29°C.

8.1 Clues from the results

First the model shows (Fig. 3) that in the equatorial band, water with an average temperature of over 28°C often propagates eastward across the Pacific but the speed is such that, in the strongest El Niños, it takes most of a year for the water to cross from west to east across the ocean.

5   In the past it has been suggested that the ocean heat involved in an El Niño is transported eastwards by one or more equatorial Kelvin waves. However this seems unlikely as simple waves does not advect heat. It would only be possible if the waves had the character of a highly non-linear tidal bore running along the shallow equatorial thermocline. Despite the amount of experimental research carried out in the area there appears to be no evidence for such waves.

It has also been suggested that such waves are generated late in the year by westerly wind bursts in the Western Pacific. The
10   model results show that although strong wind events are seen in the Western Pacific in late 1982, the main pulse of warm water started propagating eastwards much earlier in the year.

When the model archive is used to determine where heat is being transported (Fig. 5), it shows that in 1982 this occurred north of the Equator at the latitude of the NECC. The plots of sea surface temperature (Fig. 11) also emphasized the important role of the NECC.

15   This raises the question as to why the NECC is not a major transporter of heat every year? Part of the answer is that the NECC is limited to the top 300 m of ocean and that this is also the region affected the Ekman transport, the geostrophic inflow into the Equator and tropical instability waves.

A comparison of fluxes showed that over, say twenty to thirty degrees of longitude, the Ekman transport and geostrophic inflow can both seriously dilute the temperature of the water in the NECC. The mixing due to tropical instability waves is also significant and, when present, is most likely the dominant term.

During 1982, as the El Niño progressed eastward, a region of low wind and low Ekman transport developed in the Central Equatorial Pacific. The strength of the tropical instability waves also dropped significantly as did possibly due to a reduced or reversed Equatorial Current. The geostrophic inflow also reduced but this may have been due to a stronger than normal annual wave propagating westwards across the ocean.

As a result of these changes the NECC advected warm water further eastwards than normal, past the main convective region in the atmosphere. This would stimulate atmospheric convection to the east, the process being repeated leading to the propagation of the El Niño eastwards across the ocean.

Support for this comes from observations of high reflective clouds reported by Ramage (1975) and the distribution of rainfall reported by Linsley et al. (2006), rainfall also being an indicator of atmospehric convection regions. Ramage (1975) showed that during the 1971-72 El Niño the North Pacific Inter-tropical Convergence Zone moved closer to the Equator and that in December 1972, between 200°E and 240°E, it lay along a line near 6°N. The rainfall distribution also shows high rainfall in a band around 6°N in the Eastern Pacific. As seen in Fig. 11 this corresponds to the expected path of the NECC.

But again, why does this not happen every year? One clue comes from the unusually high transport in the NECC during 1982. Wyrtki (1974), using Pacific island sea level data, also reported a correlation between strong El Niño years and years with a strong NECC.

For the present model, Fig. 3 shows that there a number of years when a temperature pulse starts to move eastwards away from the Western Pacific warm pool. These may have petered out because there was not enough source water in the warm pool. However if the NECC was too weak, then as soon as the current has passed the region of maximum atmospheric convection , it could be rapidly cooled by tropical instability waves and the Ekman transport. As a result a new atmospheric convective region would not develop.

8.2 Transport along the Equator

There is one counter argument concerning this scenario and that comes from the observation that in the model a pulse of warm water is observed moving westwards along the equator during the last quarter of 1982. Initially its speed indicated that it might have the character of a tidal bore.

However the pulse only formed after the atmospheric convection region had moved further east, the total flux of the warmest waters advected by the pulse was less than that advected by the NECC and by the end of the year none of the particles had passed 240°E. As a result it is unlikely that the pulse seriously affected the further eastwards movement of the El Niño.

8.3 Hypothesis

The above scenario has only been partly justified by the analysis presented here and could do with further tests using observations and other model runs. The latter could include coupled model runs, where the advection of heat and its resulting influence on the atmosphere can be accurately tracked.

5   However despite this, the following set of hypotheses seem justified:

     1. That in reality the North Equatorial Counter Current has the potential to transport large quantities of heat away from the West Pacific Warm Pool into the Central and Western Pacific.

     2. That normally the NECC heat transport is reduced by the Ekman transport, the geostrophic inflow and tropical instability waves.

10   3. That at the longitudes of the main atmospheric convection region and to the west, the effect of these processes is reduced.

     4. That, in the right circumstances, the NECC can then transport sufficient warm pool water to the east to move the centre of the atmospheric convection region.

     5. That the 'right circumstances' include an increase in the strength of the NECC.

     6. That the increased strength of the NECC is due primarily to increased sea level along the Equator and a reduction in sea

15 level near 6°N.

     Even if the hypotheses are wrong, they provide a physical model of a developing El Niño which can be tested and if found wanting can be used to develop a better picture of the physics involved.

     They do not say what starts an El Niño event or what limits how far the convection region will move eastwards across the Pacific. These are likely to depend on the amount of warm water in the Western Pacific Warm Pool, the strength of the NECC

20 and other factors. But this is an area for future research.

     One final point. This paper has made the point that equatorial Kelvin waves, studied for example by Levine and McPhaden (2016), Chen et al. (2016) and Hu and Fedorov (2017), are unlikely by themselves to advect sufficient heat across the Pacific to move the main atmospheric convection region during an El Niño.

     The results presented here have shown that in 1982, by deepening the thermocline and raising sea level along the Equator,

25 Kelvin waves may have increased the heat advected by the NECC and so indirectly aid the development of the El Niño.

     However equally important was the reduction in the depth of the trough at 6°N, due to the annual Rossby wave, and an increase in sea level near the Equator which was not part of a equatorial Kelvin wave. The latter feature developed near the dateline, extended over ten degrees in latitude and twenty degrees in longitude, and remained fixed during much of the Autumn of 1982. It thus may be due to local heating.

30   *Code and data availability.*   At the time of publication the archived data is freely available at "http://gws-access.ceda.ac.uk/public/nemo/runs/ORCA0083-N06/means/". The Nemo ocean model code and its documentation are available from "http://forge.ipsl.jussieu.fr/nemo/wiki/Users".

Competing interests. The author is on the advisory board of Ocean Science.

5 *Acknowledgements.* I wish to acknowledge the support of the Marine Systems Modelling group and the aid of Dr Andrew Coward at the UK National Oceanography Centre, part of the Natural Environment Research Council, where much of this research was carried out. I also wish to acknowledge the earlier role of the Australian CSIRO Division of Fisheries and Oceanography. Without the financial support and the professionalism and enthusiasm of staff at both centers this work would not have been possible.

References

Barber, R. T. and Chavez, F. P.: Biological Consequences of El Niño, Science, 222(4629), 1203–1210, 1983.

Chen, S., Wu, R., Chen, W., Yu, B., and Cao, X.: Genesis of westerly wind bursts over the equatorial western Pacific during the onset of the strong 2015–2016 El Niño, Atmospheric Science Letters, 17, 384–391, 2016.

5 Cox, M.: Generation and Propagation of 30-day waves in a numerical model of the Pacific, Journal of Physical Oceanography, 10, 1168–1186, 1980.

de Vries, P. and Döös, K.: Calculating Lagrangian trajectories using time-dependent velocity fields., Journal of Atmospheric and Oceanic Technology, 18 (6), 1092–1101, 2001.

Dussin, R., Barnier, B., and Brodeau, L.: The making of Drakkar forcing set DFS5, Report 05-10-14, DRAKKAR/MyOcean, 2014.

10 Hu, S. and Fedorov, A. V.: The extreme El Niño of 2015–2016: the role of westerly and easterly wind bursts, and preconditioning by the failed 2014 event, Clymate Dynamics, pp. 1–19, https://doi.org/10.1007/s00382-017-3531-2, 2017.

Large, W. and Yeager, S.: Diurnal to Decadal Global Forcing for Ocean and Sea-Ice Models: The Data Sets and Flux Climatologies, NCAR Technical Note TN-460+STR, National Centre for Atmospheric Research, Boulder, Colorado, 2004.

Levine, A. F. Z. and McPhaden, M. J.: How the July 2014 easterly wind burst gave the 2015–2016 El Niño a head start, Geophysical Research
15 Letters, 43, 6503–6510, https://doi.org/10.1029/2005GC001115, 2016.

Linsley, B. K., Kaplan, A., Gouriou, Y., Salinger, J., deMenocal, P. B., Wellington, G. M., and Howe, S. S.: Tracking the extent of the South Pacific Convergence Zone since the early 1600s, Geochemistry, Geophysics, Geosystems, https://doi.org/10.1002/2016GL069204, 2006.

Luther, D. and Johnson, E.: Eddy energetics in the upper equatorial Pacific during the Hawaii-to-Tahiti Shuttle Experiment, Journal of Physical Oceanography, 20, 913–944, 1990.

20 Madec, G.: NEMO ocean engine (Draft edition r6039), Note du Pole de modelisation 27, Institut Pierre-Simon Laplace (IPSL), France, 2014.

McCreary, J.: A Linear Stratified Ocean Model of the Equatorial Undercurrent, Phil.Trans.R.Soc.Lond.A., 298, 603–635, 1981.

Menkes, C., Vialard, J., Kennan, S., Boulanger, J.-P., and Madec, G.: A Modeling Study of the Impact of Tropical Instability Waves on the Heat Budget of the Eastern Equatorial Pacific, Journal of Physical Oceanography, 36, 847–865, 2006.

Myers, G.: On the Annual Rossby Wave in the Tropical North Pacific Ocean, Journal of Physical Oceanography, 9, 663–674, 1979.

25 Philander, S. G. H.: Instabilities of zonal equatorial currents, Journal of Geophysical Research, 83, 3679–3682, 1978.

Ramage, C.: Preliminary discussion of the meteorology of the 1972-73 El Niño, Bulletin of the American Meteorological Society, 56, 234–242, 1975.

Stommel, H.: Wind-drift near the Equator, Deep Sea Research, 6, 298–302, https://doi.org/10.1016/0146-6313(59)90088-7, 1960.

Trenberth, K. E.: The Definition of El Nino, Bulletin of the American Meteorological Society, 78, 2771–2777, https://doi.org/10.1175/1520-
30 0477(1997)078<2771:TDOENO>2.0.CO;2, 1997.

Webb, D.: A comparison of sea surface temperatures in the Equatorial Pacific Nino regions with results from two early runs of the NEMO 1/12° Ocean Model, Research and Consultancy Report, No. 55, National Oceanography Centre, Southampton, U.K., 2016.

Wyrtki, K.: Teleconnections in the Equatorial Pacific Ocean, Science, 180(4081), 66–68, 1973.

Wyrtki, K.: Equatorial Currents in the Pacific 1950 to 1970 and Their Relation to the Trade Winds, Journal of Physical Oceanography, 4,
35 372–380, 1974.

Wyrtki, K.: El Niño - The Dynamic Response of the Equatorial Pacific Ocean to Atmospheric Forcing, Journal of Physical Oceanography, 5, 372–380, 1975.

Wyrtki, K.: Sea level During the 1972 El Niño, Journal of Physical Oceanography, 7, 779–787, 1977.

Wyrtki, K.: The Response of sea Surface Topography to the 1976 El Niño, Journal of Physical Oceanography, 9, 1224–1231, 1979.